[10]J. D. Keys, Ph.D. thesis, McGill University, 1951 (unpublished).
[11]P. A. Tove, Arkiv Fysik 13, 549 (1958).
[12]R. L. Hahn, M. F. Roche, and K. S. Toth, Nucl. Phys. A113, 206 (1968).
[13]D. F. Torgerson, R. A. Gough, and R. D. MacFarlane, Phys. Rev. 174, 1494 (1968).
[14]C. P. Ruiz, University of California Lawrence Radiation Laboratory Report No. UCRL-9511, 1961 (unpublished).
[15]S. G. Nilsson, C. F. Tsang, A. Sobiczewski, Z. Szymański, S. Wycech, G. Gustafson, I. L. Lamm, P. Möller, and B. Nilsson, Nucl. Phys. A131, 1 (1969).
[16]W. D. Myers and W. J. Swiatecki, Arkiv Fysik 36, 343 (1967).
[17]G. T. Garvey, W. J. Gerace, R. L. Jaffe, I. Talmi, and I. Kelson, Rev. Mod. Phys. 41, 1 (1969).
[18]V. E. Viola and G. T. Seaborg, J. Inorg. Nucl. Chem. 28, 697, 741 (1966).
[19]N. Zeldes, A. Grill, and A. Simievic, Kgl. Danske Videnskab. Selskab, Mat.-Fys. Medd. 3, No. 5 (1967).

PHYSICAL REVIEW C VOLUME 2, NUMBER 5 NOVEMBER 1970

Total Neutron Cross Section of Oriented ^{165}Ho from 2 to 135 MeV*

H. Marshak
National Bureau of Standards, Washington, D. C. 20234

and

A. Langsford
Atomic Energy Research Establishment, Harwell, Didcot, Berkshire, England

and

T. Tamura†
Oak Ridge National Laboratory, Oak Ridge, Tennessee 37830 and University of Texas, Austin, Texas 78712

and

C. Y. Wong†
Oak Ridge National Laboratory, Oak Ridge, Tennessee 37830
(Received 17 June 1970)

The difference in the total neutron cross section due to nuclear orientation, $\Delta\sigma_{def}$, has been measured for ^{165}Ho over the energy range of 2 to 135 MeV. The results show that $\Delta\sigma_{def}$ oscillates as well as changing sign, contrary to our classical concept of the interaction. The data, both σ_t and $\Delta\sigma_{def}$, are successfully fitted by adiabatic coupled-channel calculations using the optical model. The parameters for the optical model were determined by fitting σ_t and σ_R data (over approximately the same energy range as in the present work) for the two spherical nuclei Cd and Pb. The only additional quantity introduced was the quadrupole deformation parameter for ^{165}Ho which is known to be 0.33. The data for $\Delta\sigma_{def}$ can also be explained quite well by a simple semiempirical model which makes use of the black-nucleus model, the nuclear Ramsauer effect, and the experimental σ_t data. The temperature dependence of $\Delta\sigma_{def}$ agrees very well with our calculated values for the degree of nuclear orientation, which is consistent with ^{165}Ho being almost a pure quadrupole-shaped nucleus.

I. INTRODUCTION

In order to study the effect on the total neutron cross section of changing the spatial orientation of a deformed nucleus, holmium-165 plays a unique role, since it is a highly deformed nucleus which occurs monistopically and can be easily oriented.[1] This effect is called the nuclear-deformation effect, $\Delta\sigma_{def}$, and it is defined as the difference in the total neutron cross section due to nuclear orientation; $\Delta\sigma_{def} = \sigma_t(\text{oriented}) - \sigma_t(\text{unoriented})$. It was first measured for ^{165}Ho by Wagner *et al.*[2] using 0.35-MeV neutrons. Subsequent measurements were also made on ^{165}Ho at neutron energies of 14 MeV[3] and at 8 and 15 MeV.[4]

If one considers the interaction of a neutron with the prolate-shaped holmium nucleus in the framework of the black-nucleus model,[5] the *sign* of $\Delta\sigma_{def}$ would always be positive if the nucleus were oriented perpendicular to the neutron beam, and negative if it were oriented parallel to the neutron beam. Of course, one should not expect this simple model to be valid at the neutron energies used in the above four measurements, since the relation

$kR \gg 1$ is not yet valid.[6] Furthermore, the total cross section of ^{165}Ho was known up to 15 MeV[7] and was not a monotonically decreasing function as the black-nucleus model predicts, viz., $\sigma_t = 2\pi(R+\lambda\!\!\!^{-})^2$.

In contrast, the optical model should be quite useful in understanding the nuclear-deformation effect. Using this model, a distorted-wave Born approximation (DWBA) calculation[8] of $\Delta\sigma_{def}$ was made for neutrons of 2, 5, and 14 MeV before any experimental results were obtained. The results of this calculation showed that the value of $\Delta\sigma_{def}$ at 5 MeV was of opposite sign to that predicted by the black-nucleus model. A detailed analysis of $\Delta\sigma_{def}$ using the adiabatic coupled-channel (ACC) calculation[9] covering the energy range of 0.35 to 15 MeV was reported with the 8- and 15-MeV experimental results.[4] This calculation, using reasonable values for the optical-model parameters, fitted these two experimental points, as well as the 0.35- and 14-MeV points previously measured. It also showed that $\Delta\sigma_{def}$ undergoes an oscillation as well as a sign change, with the latter taking place between approximately 2 and 7 MeV. Thus, although the magnitude and sign of $\Delta\sigma_{def}$ for the four measured values [two (0.35 and 14 MeV) with the nuclei oriented perpendicular to the beam and the other two with the nuclei oriented parallel to the beam] were in good agreement with the ACC calculation, the *signs* of all four values were also in agreement with the predictions of the black-nucleus model. It would, therefore, seem worthwhile to make further measurements of $\Delta\sigma_{def}$ in this energy range in order to verify the sign change and oscillation predicted by the ACC calculation. One can also raise the questions: Does the ACC calculation predict further oscillations in $\Delta\sigma_{def}$ at higher neutron energies (>15 MeV) and can they be experimentally verified?

Although the total neutron cross section for holmium was not measured above 15 MeV at the outset of this work, it was known that it should exhibit broad maxima and minima as a function of energy. Measurements made of other nuclei covering an energy range of up to 120 MeV have shown this behavior.[10] In fact, the experimental evidence is that there are three continuous families of broad maxima and minima in the total neutron nuclear cross sections (we are ignoring the broad maximum which appears at much higher energies, 1.5 to 2 GeV) and furthermore these shift to higher energies as the mass number (and thus the radius) of the target is increased. The interpretation of these has been made by Lawson[11] in terms of interference effects between the neutron wave going through and around the nucleus. A more detailed analysis was made by Peterson[12] who showed that one could interpret these broad maxima and minima in an analogous fashion to the Ramsauer effect in the low-energy scattering of electrons by noble gases; hence the name "nuclear Ramsauer effect." McVoy[13] and Franco[14] have discussed these phenomena further.

Since the ACC calculation predicts that $\Delta\sigma_{def}$ undergoes an oscillation with a sign change in the energy region <15 MeV (with perhaps further oscillations at higher energies) and the black-nucleus model does not, we would want to dismiss it completely in understanding this effect. If we keep in mind, however, that experimentally the maxima and minima in the total cross section move towards higher (or lower) neutron energies as we increase (or decrease) the radius of the target nucleus, then we must take this into account when we orient a deformed nucleus. Thus, the following two-step semiemperical model can be evolved in an attempt to understand the behavior of $\Delta\sigma_{def}$ in a simple way: First, there is a decrease in the total cross section of the target when we orient the prolate nucleus with its symmetry axis along the beam direction. This reduction in the total cross section is just the amount calculated using the black-nucleus model. Second, there is a corresponding increase in the effective path length of the nucleus which causes the maxima and minima in the total cross section to shift to higher energies. The details of this model are described in Sec. VI of this paper. It is rather obvious that the resulting σ_t(oriented) curve calculated using this model would be similar to the experimentally determined σ_t(unoriented) curve, but depressed by the black-nucleus amount and shifted slightly to higher energies. Upon subtracting these two curves to obtain $\Delta\sigma_{def}$ one gets a curve which would oscillate and go negative under the right conditions. Since, as we mentioned previously, the total cross section of ^{165}Ho has been measured up to 15 MeV, we can make an exact calculation of $\Delta\sigma_{def}$ using this semiempirical model and compare these results to those of the ACC calculation.[4] However, we would still only be able to compare these to the four measurements made of $\Delta\sigma_{def}$.

Although it would be useful to make more measurements of $\Delta\sigma_{def}$ over this energy range, it would be worthwhile to also extend the measurements to as high a neutron energy as possible. This, of course, should be accompanied by a complete theoretical analysis of $\Delta\sigma_{def}$ using the ACC calculation as well as seeing if our semiemperical model is valid. Thus the present work, which consisted of experimentally determining $\Delta\sigma_{def}$ over an energy range of 2 to 135 MeV along with the theoretical analyses, was undertaken.

Since the only existing facility to carry out these

total-neutron-cross-section measurements was at the Atomic Energy Research Establishment (AERE) Laboratory, Harwell, England, the National Bureau of Standards ^{3}He refrigerator was shipped there. In Sec. II A this facility and the experimental arrangement are described. As our ^{165}Ho single crystal[2,3] was too thin for these new measurements and no thicker one was available, we used a thick polycrystalline sample in a similar manner to Ref. 4. The new cryostat, which had to be built to incorporate a large superconducting solenoid mounted at right angles to the vertical axis of the cryostat is described in Sec. II B.

In our discussion so far we have treated the ^{165}Ho nucleus[15] as if it were a pure prolate quadrupole, and although some evidence existed for this, no definitive experiment was done until Hendrie *et al.*[16] measured the higher-order components in the shapes of the rare-earth nuclei by α scattering. Our results, which were analyzed about the time that their results became available, can be shown to be consistent with the assumption that the shape of the ^{165}Ho is very nearly pure quadrupole. Since this conclusion depends intimately on the values for the nuclear-orientation parameters,[17] which in turn depend upon the model used for the atomic magnetization of ^{165}Ho, we present the calculation of these parameters in detail in Sec. III. The experimental results are presented in Sec. IV. In Sec. V the theoretical analysis is given in terms of coupled-channel calculations, while Sec. VI gives theoretical arguments based on the black-nucleus model and the nuclear Ramsauer effect. The conclusions are given in Sec. VII.

II. EXPERIMENTAL ARRANGEMENT

A. Neutron Facility and Experimental Procedure

Measurements of the total neutron cross section and the nuclear-deformation effect for ^{165}Ho were made over the energy range of 2 to 135 MeV using the neutron time-of-flight spectrometer[18] associated with the Harwell synchrocyclotron.

The method used for the total-cross-section measurement was similar to that previously employed for σ_t measurements on other elements[10] using this apparatus; i.e., the determination of the attenuation of a sample of holmium placed in a collimated neutron beam in good geometry. Although the layout of the apparatus for the measurements of σ_t was almost identical to that used in the measurements of $\Delta\sigma_{def}$, which is shown in Fig. 1, the following differences should be noted: The flight path was 27 m long and the holmium sample was placed on a sample changer which was arranged to move it into and out of the beam at 200-sec intervals. Also the present arrangement of monitor detectors which were placed in the defined neutron beam on the upstream side of the sample is different from that described earlier.[18] Two monitor detectors were used in order to check monitor stability. Since the sample was frequently moved into and out of the beam, errors arising from fluctuations in counting rate due to fluctuations in the counter thresholds were thus very much reduced. The small variation which did occur during the experiment produced negligible error in the total cross section. Main and monitor detectors were plastic scintillators viewed by 14-stage fast-response photomultipliers, their acceptance thresholds set with respect to the Compton recoil edge produced by irradiating the detectors with γ rays from a ^{137}Cs source.

The neutron beam, defined by collimators C_1 and C_2 in Fig. 1, was 1.27 cm square at the holmium sample. The holmium sample was a right circular cylinder 6.998 cm long and 2.229 cm in diameter. Its areal density was 2.261×10^{23} atoms/cm^2. The total data-collection time was 9 h for σ_t.

The experimental technique employed to obtain $\Delta\sigma_{def}$ for holmium was broadly similar. The method compared the intensity of neutrons transmitted through the sample when it was oriented (e.g., at 0.32 K and $H = 50$ kOe) with that when unoriented (4.2 K and $H = 50$ kOe). For convenience we shall describe measurements made at these two temperatures as "cold" and "warm," respectively.

The holmium sample used for these measurements was of the same diameter as that used in the σ_t measurements, but 11.942 cm long. Both samples came from the same ingot, which was 99.9% pure. They were also radiographed to insure being void free.

The change in total cross section, and hence in intensity, was expected to be small, especially at certain energies (e.g., around 8 MeV, see Ref. 4) and so it was necessary to pay strict attention to detector stability and monitoring, particularly as the experimental conditions could not be rapidly changed. It took about 1.5 h to cool the sample.

The change of experimental area to the 20-m flight path (see Fig. 1), to accommodate the large ^{3}He refrigerator introduced a small background of high-energy neutrons filtering through the shielding wall. This was measured by placing a 1-m brass shadow bar between the holmium sample and the main counter to block the direct neutrons. Measurements were made for both "warm" and "cold" runs.

The measurement of $\Delta\sigma_{def}$ was done in two stages; first, a series of seven independent data sets was made with the superconducting solenoid switched off and then another series of seven more with it switched on. Each independent data set

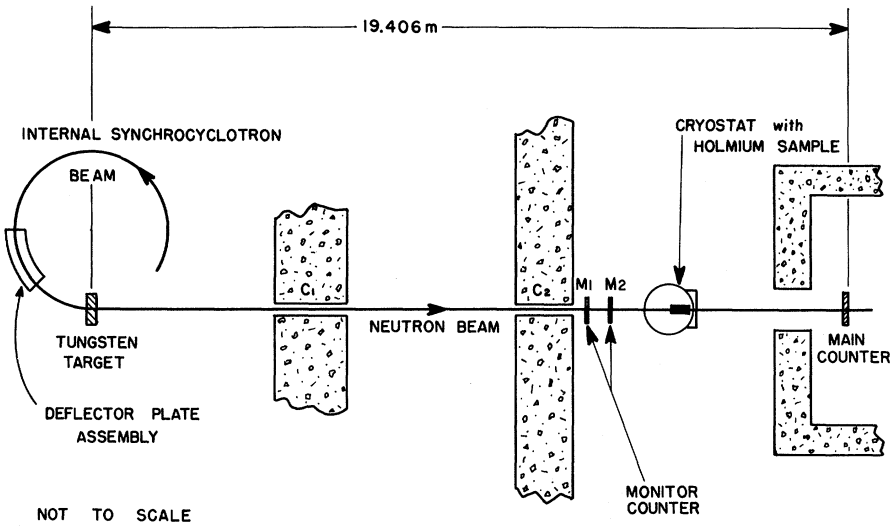

FIG. 1. The experimental arrangement. The direction of nuclear orientation was along the beam direction.

consisted of a 12-h measurement of the normalized transmitted neutron energy spectrum plus a 1-h background with the sample "cold," and then the entire procedure repeated with the sample "warm." The over-all statistical uncertainties in each series were determined by their self-consistency. In zero magnetic field there can, of course, be no nuclear orientation at any temperature in a polycrystalline sample. Thus the "field-off" series served to establish whether there was any intensity change produced merely by the systematic effect of changing the temperature. A small effect, which was not strongly energy dependent, was found for the "field-off" series taken at 0.32 K. This was subtracted from the relatively larger and energy-dependent "field-on" series to obtain our final $\Delta\sigma_{def}$ results. The small effect found for the "field-off" series was attributed to a slight misalignment of our sample. A similar series of data sets was also made for 0.37 K after a careful realignment of our sample. This time the "field-off" data showed no effect. The result of all these measurements as well as those at other temperatures are given in a later section.

In order to acheive high stability in the detectors, weak ^{137}Cs sources were placed near each one. Their presence introduced a well-known but almost vanishingly small background to the neutrons detected during the neutron pulse. The background was, however, monitored on scalers which were gated off during the neutron pulse. It was established experimentally that the variation of background counting rate was 50 times more sensitive to changes in detector gain than was the neutron counting rate. Corrections to the monitored beam intensity were applied which took into account the small change in background count rate measured by the monitor counter. Typical changes in background count rate were about ±10%, implying a ±0.2% change in the number of neutrons detected. This corresponded to a systematic error, due to monitoring, of ±5 mb. The consistency of source counter rate for the main counter showed that it was significantly more stable than the monitor system, thus eliminating the need to make any corrections to the main-detector counting rate.

B. Oriented ^{165}Ho Target

The oriented ^{165}Ho target used in the present measurements of $\Delta\sigma_{def}$ was a thick polycrystalline sample rather than the single crystal we used in our previous work. Although a single-crystal sample is more advantageous, as one can obtain a high degree of nuclear alignment[19] without a magnetic field, no thick single crystal was available. We therefore used a somewhat similar target arrangement to that used in Ref. 4, namely a long cylindrical polycrystalline sample cooled to pumped ^{3}He temperatures in a magnetic field. In order to do this a new cryostat, Fig. 2, was built for the National Bureau of Standards ^{3}He refrigerator[20] which incorporated a relatively high-field superconducting solenoid mounted at right angles to its vertical axis.[21] This cryostat was designed to operate for long periods (>48 h) at low temperatures without retransferring liquid helium. In addition, the "working end" (^{3}He-cooled region) was kept simple enough so that various experimental arrangements could be accomplished with minor modifications.

Since the degree of nuclear orientation obtained for a polycrystalline ^{165}Ho sample depends upon the temperature and magnetization achieved, and

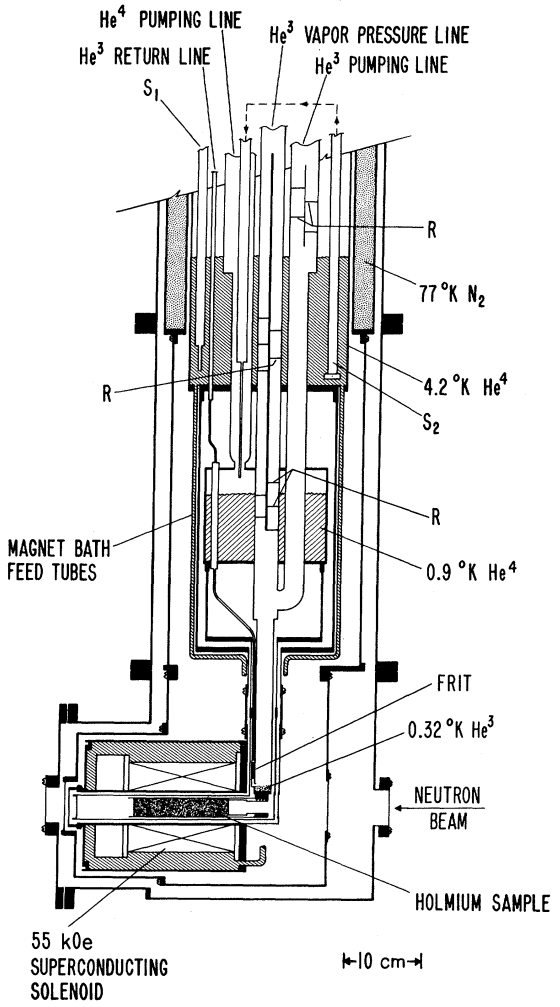

FIG. 2. Schematic view of ^{3}He cryostat.

whereas the former cannot be readily changed,[22] the latter can be substantially increased over the 18 kG[23] used in Ref. 4; this corresponds to 70% of saturation magnetization, $\mathfrak{M}/\mathfrak{M}_\infty = 0.07$. At the time this work was undertaken no reliable magnetization data above 26 kG existed for polycrystalline holmium[24]; however, enough was known about the magnetic properties of single crystals to make some general predictions about those of a polycrystalline sample. This is discussed in detail in the following section, so we shall only state the salient points here – namely, that the magnetization should reach an intermediate saturation plateau of $\mathfrak{M}/\mathfrak{M}_\infty \simeq 0.8$ at about 40 kG and then rise rather slowly with full saturation not expected till fields of the order of hundreds of kG are applied. Since superconducting solenoids with sufficient fields for full saturation are not readily available, it was decided to use one that at least enabled the sample to be in the intermediate saturation region.

A schematic drawing of the lower part of the ^{3}He cryostat is shown in Fig. 2. It has two liquid-nitrogen baths, the main one, which is shown in the drawing, has a capacity of 16 liters and a secondary one located near the top of the cryostat has a capacity of only 3.5 liters. Whereas the main bath and its extended copper radiation shield serve the usual purpose, the secondary bath serves as both a radiation trap and a thermal ground at 77 K for all the tubes going into and making up the main ^{4}He bath. The latter has a capacity of 20 liters. The pumped ^{4}He bath has a capacity of 1.6 liters and serves both to liquefy the returning ^{3}He gas and as a 0.9-K radiation shield surrounding the ^{3}He tail and holmium sample. The various tubes for pumping on the ^{4}He bath and for pumping and recirculating ^{3}He are shown in this drawing. Some of the radiation shields in these tubes are labeled R. The frit is a porous, stainless-steel plug which is used to restrict the ^{3}He flow rate. S_1 is the main transfer syphon. S_2 is a smaller syphon connecting the main ^{4}He bath to the pumped ^{4}He bath and allows us to transfer liquid helium during the main transfer as well as retransferring at a later time.

The superconducting solenoid we used could be operated as high as 55 kG (center field) in the persistent mode without going normal. It has an i.d. of 4.45 cm, an o.d. of 12.70 cm, and is 12.70 cm long. At full field the stored energy is 5.1 kJ. Because of the large amount of stored energy and to facilitate the cool down, the solenoid was mounted in its own 4.2-K liquid-helium bath, Fig. 2, rather than in the vacuum space as in Ref. 4. This bath holds 1.2 liters and is connected to the main 4.2-K bath by three 1.27-cm-diam tubes. These tubes are offset so as not to be in the way of the neutron beam. One of these tubes also contains the power and persistent switch leads going from the solenoid to a connector in the bottom of the main 4.2-K bath. Removable leads are used from this connector to the top of the cryostat in order to reduce the h at leak into the main 4.2-K bath when the solenoid is operated in the presistent mode. A 1-Ω 10-W resistor which shunts the power leads is located near the connector in the main 4.2-K bath to help dissipate some of the energy away from the small magnet bath if the solenoid should accidentally go normal. One of the remaining two tubes also has in it a 3.1-mm Teflon tube which goes from the bottom of the syphon S_1 to the very bottom of the magnet bath. This serves a dual purpose – first, to remove all of the liquid nitrogen which is used in precooling; and second, to yield a greater transfer efficiency in filling the magnet and main ^{4}He bath with liquid helium.

The total time required to cool the sample from room temperature to 0.32 K was approximately 4 h

with about 1.5 h needed to go from 0.9 to 0.32 K (^{3}He cooling cycle). The relatively long time it takes for the last part of our cooling cycle is not unreasonable considering the very large nuclear Schottky anomaly in the specific-heat curve of holmium in this temperature region and the large mass (412.2 g) of our sample.[25] In order to insure good thermal contact between the ^{3}He tail and the holmium sample, it is first soldered[26] into a copper[27] tube which is threaded on one end; this is then screwed into a copper holder which makes up the lower part of the ^{3}He tail. The bottom surface of the inside of the ^{3}He tail has been substantially increased to reduce the "Kapitza resistance." Apiezon-*N* grease is used to make thermal contact at the threaded joint.[28] Owing to the right-angle geometry of the bottom of the cryostat, the sample can be put in by simply removing the thin[29] windows in the radiation shields along the beam path. This geometry is also very convenient for lining up the holmium sample with the neutron collimator, as all that is necessary is to remove the thin windows and use standard visual techniques.[30]

The temperature of the sample was determined by two calibrated 470-Ω carbon Speer resistors, one located in the copper part of the ^{3}He tail and the other in the front face of the sample (out of the neutron beam). These resistors were calibrated against the ^{3}He vapor-pressure scale. This was done in zero magnetic field and also as a function of field, since it is known that carbon resistors have a small magnetoresistive effect. The uncertainty in the temperature measurement is estimated to be less than ±10 mK.

III. NUCLEAR ORIENTATION OF ^{165}Ho

Although one can obtain a very high degree of nuclear orientation for holmium metal because of the extremely large hyperfine interaction[31] and favorable low-temperature magnetic properties,[32] the exact values for the orientation parameters can only be calculated if the sample is magnetically saturated. The reason for this is that the symmetry axis of the nuclear spin coincides with the direction of the atomic moment. In the case of magnetic saturation, the only quantities entering the calculation are the hyperfine and quadrupole coupling constants. The latter are quite small[33] and can be neglected with little effect on the final values for the orientation parameters. If the sample is a single crystal, magnetic saturation can be achieved at fairly low fields[34] (the order of kilogauss for an easy direction of magnetization). When the sample is a polycrystal, magnetic saturation can only be achieved at very high fields[35] (the order of hundreds of kilogauss). For the case where the sample, either single crystal or polycrystal, is not magnetically saturated, one has to know the distribution of atomic moments in order to calculate the exact values for the orientation parameters. Although there is considerable information on the low-temperature magnetic properties of holmium metal, especially for single crystals, the exact distribution of atomic moments as a function of applied field is not known. Magnetization measurements have been made, but these only give one information related to the first orientation parameter – the nuclear polarization. Experiments can be performed to measure the higher-order orientation parameters; however, none has been done using a polycrystalline sample.[36] The present experiment, under certain assumptions as to the multipole order needed to define the nuclear shape, uniquely determines the second orientation parameter – the nuclear alignment. Therefore, it would be worthwhile to outline the calculation of the nuclear orientation parameters for a polycrystalline sample as used in the present experiment.

This calculation has been described previously in Ref. 4 and in greater detail in the thesis of Shelley.[37] Our discussion will not go into all the details – just the relevant parts – and will point out the slight difference in the magnetic model we used in calculating the orientation parameters. For ease of comparison with Ref. 4, we shall use the same notation (namely – the so-called statistical tensors) rather than the orientation parameters as defined by Tolhoek and Cox, which were used in our previous papers.

For a nuclear-spin system with axial symmetry the statistical tensors B_K are defined as follows:

$$B_K=(2I+1)^{1/2}\sum_M P_M(-)^{I-M}(IMI-M|K0)\,, \qquad (3.1)$$

where I is the nuclear spin, M the magnetic quantum number, P_M the occupational probability of the Mth magnetic substate, and $0\leq K\leq 2I$.

If all the atomic moments are lined up in one direction, as they would be for a magnetically saturated sample (that is, when the ratio of the magnetization $\mathfrak{M}$ of the sample to the saturation magnetization $\mathfrak{M}_\infty$ is unity) then the statistical tensors can be determined by simply calculating the P_M's. The ground-state splitting for holmium metal can be represented by using the following spin Hamiltonian with effective spin $S=\frac{1}{2}$:

$$\mathcal{H}=AS_zI_z+P[I_z^2-\tfrac{1}{3}I(I+1)]\,, \qquad (3.2)$$

where the direction of the applied field is along the z axis, I_z is the projection of the nuclear-spin operator I on this axis, and the quantities A and P represent the strengths of the dipole and quadrupole interactions, respectively. The eigenvalues

for this Hamiltonian are given by the expression

$$E_M = \pm\tfrac{1}{2}AM + P[M^2 - \tfrac{1}{3}I(I+1)]\,. \tag{3.3}$$

For the case under discussion, that is, where $\mathfrak{M}/\mathfrak{M}_\infty = 1$, only the lowest electronic state ($S_z = \frac{1}{2}$) is occupied. The sign of the dipole constant is positive, and thus the lowest magnetic substate is $M = +\frac{7}{2}$; that is, the nuclei are polarized in the direction of the applied field. The best values for the dipole and quadrupole constants come from the specific-heat measurements,[33] and they yield $A/k = 0.64 \pm 0.01$ K and $P/k = 0.007 \pm 0.0015$ K, where k is the Boltzman constant. Since the energy levels E_M can now be calculated, the P_M's are obtained as a function of temperature by using the Boltzman factor, viz.,

$$P_M = e^{-E_M/kT} / \sum_M e^{-E_M/kT}\,. \tag{3.4}$$

The statistical tensors for this case of complete magnetic saturation can be calculated directly as a function of temperature.

For the case where we do not have magnetic saturation and the atomic moments are distributed symmetrically around the field direction, the statistical tensors B_K' can be calculated from the following relation:

$$B_K' = B_K \langle P_K(\cos\theta)\rangle \tag{3.5}$$

with

$$\langle P_K(\cos\theta)\rangle = \int_0^\pi P_K(\cos\theta) W(\theta) d\theta\,. \tag{3.6}$$

Here $P_K(\cos\theta)$ is the Kth order Legendre polynomial, θ is the angle between an atomic moment and the field direction, and $W(\theta)$ is the distribution of atomic moments, which is a function of the applied field. Although $\langle P_1(\cos\theta)\rangle$ is just $\mathfrak{M}/\mathfrak{M}_\infty$, the higher-order magnetic moments [$K > 1$ in (3.6)] depend upon the exact distribution $W(\theta)$.

Since this function $W(\theta)$ is not known, we have to use some model for the distribution of atomic moments versus the applied field for polycrystalline holmium metal in order to calculate the statistical tensors B_K'. The model we used to calculate $\langle P_K(\cos\theta)\rangle$ was almost the same as that used in Ref. 4; we treat polycrystalline metal as being composed of randomly oriented, noninteracting single crystals whose atomic moments exhibit the behavior predicted by neutron diffraction and magnetization measurements. Such a model would show an intermediate saturation plateau in the magnetization curve at relatively moderate fields. The values for $\langle P_K(\cos\theta)\rangle$ at this saturation plateau can be calculated from the following expression:

$$\langle P_K(\cos\theta)\rangle_{\text{sat}} = \frac{6}{\pi}\int_0^{80^\circ} d\theta' \int_0^{\pi/6} \sin\theta' P_K(\cos\theta_1) d\varphi' + \frac{6}{\pi}\int_{80^\circ}^{\pi/2} d\theta' \int_0^{\pi/6} \sin\varphi' P_K(\cos\theta_2) d\varphi'\,, \tag{3.7}$$

where

$$\cos\theta_1 = \cos\theta'\cos\theta_0 + \sin\theta'\sin\theta_0\cos\varphi'\,, \quad \theta_0 = 80^\circ\,,$$

and

$$\cos\theta_2 = \cos^2\theta' + \sin^2\theta'\cos\varphi'\,.$$

The angle θ' is between the field direction and the c axis of a crystallite, and the angle φ' is between the b axis (easy direction of magnetization) that is closest to the field direction and the greatest projection of the field on the basal plane.

At saturation in this model we have (1) for those crystallites with angle $\theta' \leq 80^\circ$ the atomic moments are all lined up in one direction and lie on the plane defined by the c axis and the b axis closest to the field and canted out of the basal plane by 10°, and (2) for those crystallites whose c axis is >80° to the field direction the atomic moments are no longer canted out of the basal plane by 10° but this angle is reduced and, in fact, θ_0 then changes as θ'. The first double integral in (3.7) corresponds to (1) and the second double integral corresponds to (2). The model used in Ref. 4 is the first double integral but with the upper limit being 90° instead of 80°. Although our model is closer to the observed data (for example, if $\theta' = \pi/2$, then the atomic moments lie in the basal plane and along an easy direction of magnetization, *not* canted out of the basal plane by 10°), the differences between our values and their values of $\langle P_K(\cos\theta)\rangle_{\text{sat}}$ were small [$\langle P_1(\cos\theta)\rangle_{\text{sat}}$ was 0.826 for our model and 0.825 for theirs]. Since the value of $\langle P_1(\cos\theta)\rangle_{\text{sat}}$ is a measurable quantity, that is, we should see some sort of intermediate saturation plateau in the experimental magnetization curve, a check on this model would be to measure $\mathfrak{M}/\mathfrak{M}_\infty$ to fairly high fields. In Fig. 3 we see the results of magnetization measurements made on polycrystalline holmium metal at the National Magnet Laboratory.[38] The spherical sample used for these measurements was cut from an unused part of our original holmium sample. As one can see from this curve, the magnetization rises rapidly at first ($B_0 < \sim 20$ kG) and then increases rather slowly. In particular, the magnetization does seem to level off, or at least rises very slowly after 50 kG; the value at 50 kG is 0.825, whereas at 60 kG it is only 0.835. These values, indicating an intermediate magnetization saturation in polycrystalline holmium, are in good agreement with the model.[39]

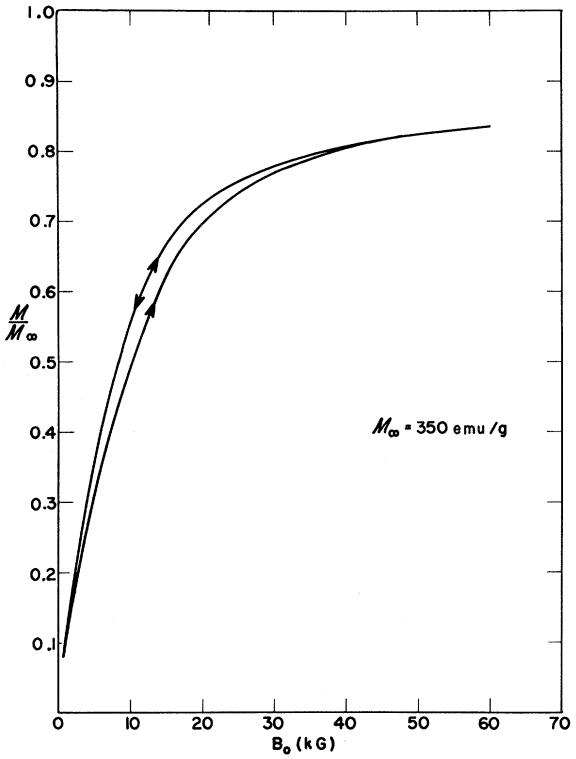

FIG. 3. 4.2-K magnetization curve for polycrystalline holmium metal.

Although the field at the center of the superconducting solenoid was 50 kOe for most of the neutron measurements, the internal field averaged over the entire sample (and subtracting out the demagnetizing field) was 40 kOe, This corresponds to a value of 0.80 for $\mathfrak{M}/\mathfrak{M}_\infty$. Since this is less than the saturation magnetization value predicted by the model, we assumed (as in Ref. 4) that the resulting statistical tensors were reduced accordingly; that is, (0.03/0.83) of our sample was composed of crystals which were completely unmagnetized. The values for the B_K' were then calculated as a function of temperature using (3.5) and with $\langle P_K(\cos\theta)\rangle = (0.80/0.83)\langle P_K(\cos\theta)\rangle_{\text{sat}}$. These are listed in Table I along with their normalized values $B_K'/B_K(\max)$ for $K=0$ to 4 and for one of the particular temperatures (0.32 K) used in the measurements. The corresponding values for the case of complete magnetic saturation, B_K and $B_K/B_K(\max)$, have also been listed. In both cases the higher K values ($K=5$, 6, and 7) are insignificantly small and have therefore been neglected. Although it will be shown later in the theoretical section that the coupled-channel equations can be written in terms of statistical tensors, and as one would expect in terms of only the even K values, the existing program is in terms of the magnetic populations. These are obtained from the

TABLE I. Statistical tensors B_K and B_K' for a polycrystalline holmium sample at 0.32 K. B_K is for the case where $\mathfrak{M}/\mathfrak{M}_\infty = 1$ and B_K' where $\mathfrak{M}/\mathfrak{M}_\infty = 0.8$.

K	B_K	$\langle P_K(\cos\theta)\rangle$	B_K'	$B_K/B_K(\max)$	$B_K'/B_K(\max)$
0	1	1	1	1	1
1	1.24	0.80	0.99	0.81	0.65
2	0.835	0.55	0.46	0.55	0.30
3	0.379	0.32	0.12	0.31	0.10
4	0.121	0.173	0.021	0.15	0.03

following expression:

$$P_M' = (2I+1)^{-1/2}\sum_K B_K'(-1)^{I-M}(IMI-M|K0). \quad (3.8)$$

For the case of incomplete magnetic saturation, the values we obtain for the B_K' depend, of course, on the model we used for the magnetization. This is shown in Fig. 4 where we plotted $B_2/B_2(\max)$ and $B_2'/B_2(\max)$ as a function of the reciprocal of the temperature. As one can see from this figure, the value of $B_2'/B_2(\max)$ is considerably less than $B_2/B_2(\max)$. Although $B_2/B_2(\max)$ tends towards unity as it should, $B_2'/B_2(\max)$ never reaches unity, even at absolute zero. Its maximum value is 0.567.[40] A measurement of the nuclear-deformation effect as a function of temperature should fit on the $B_2'/B_2(\max)$ curve if our magnetic model is correct. The only correction we might have to make is to include the $B_4'/B_4(\max)$ contribution if it were large. Since in our magnetic model $B_4'/B_4(\max)$ is small, the only way the contribution could be significant is if the nuclear-shape parameter, viz.,

$$R = R_0(1+\beta_2 Y_{20}+\beta_4 Y_{40}+\beta_6 Y_{60}) \quad (3.9)$$

had a large β_4 contribution. Fortunately it turns out[16] that β_4 (as well as β_6) is very small, that is, ^{165}Ho is very nearly a pure quadrupole-shaped nucleus.

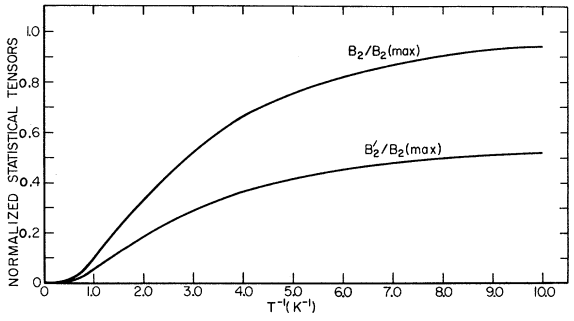

FIG. 4. Calculated degree of nuclear alignment for ^{165}Ho. $B_2/B_2(\max)$ corresponds to the case of complete magnetic saturation; $\mathfrak{M}/\mathfrak{M}_\infty = 1$, and the $B_2'/B_2(\max)$ corresponds to our experimental conditions; $\mathfrak{M}/\mathfrak{M}_\infty = 0.80$.

We did not include any uncertainties in the values of B_K' in Table I. These would arise from uncertainties in both B_K and $\langle P_K(\cos\theta)\rangle$. The uncertainties in B_K can be calculated from the uncertainties in A, P, and our sample temperature. These turn out to be relatively small when compared with the uncertainties in $\langle P_K(\cos\theta)\rangle$. Some idea of the uncertainty in the $K=1$ term can be obtained, since it is just $\mathfrak{M}/\mathfrak{M}_\infty$ of our sample. If we assigned an uncertainty of ± 0.02 to our magnetization value of 0.80, this would imply that our final field could be in error by as much as -10 or $+7$ kOe, which is quite pessimistic.[41] Uncertainties in the higher values of $\langle P_K(\cos\theta)\rangle$ are difficult to estimate, since changes in the magnetic model affect the higher terms in K progressively more; for example, comparing our model with that of Ref. 4, the difference in the $K=1$ term was 0.1% whereas the next three terms differed by 0.4, 1.3, and 3.6%, respectively. Thus if we assigned a 2% error in our $K=1$ term, we could have as much as a 70% error in the $K=4$ term. Since the $K=2$ term is the most relevant in the present experiment, a reasonable estimate of the uncertainty in it is about 10%.[42]

IV. EXPERIMENTAL RESULTS

A. Total Neutron Cross Section

In Fig. 5 we show the results of our total neutron cross-section measurements for ^{165}Ho covering an energy range from 1 to 135 MeV. The error bars are due to counting statistics alone. Our data are in very good agreement with the five discrete energy points; 1 and 1.1 MeV,[43] 8 and 15 MeV,[4] and 14 MeV,[3] previously measured (these are shown in Fig. 5). The over-all agreement with the data of Foster and Glasgow,[7] covering an energy range of 2.5 to 15 MeV, is excellent. We did not include these in Fig. 5, since there were too many data points.

B. Deformation Effect

The results of measuring $\Delta\sigma_{\rm def}$ from 2 to 135 MeV are shown in Fig. 6. These data were taken at a temperature of 0.32 K and the value of $B_2'/B_2(\max)$ was 0.30. The error shown for each point

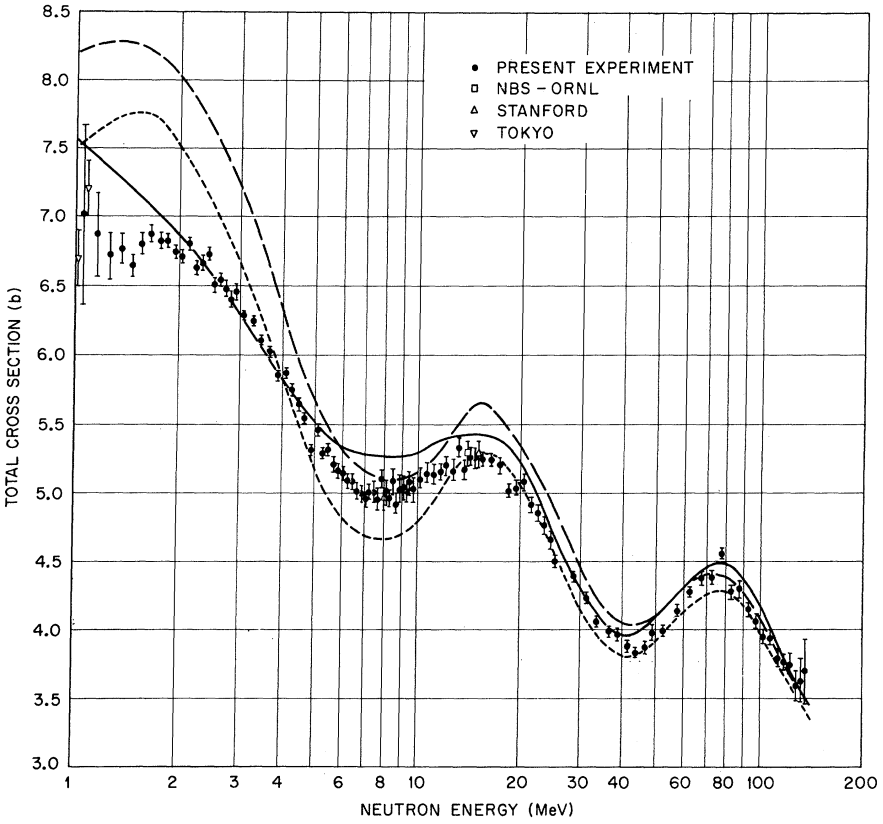

FIG. 5. Total neutron cross section for ^{165}Ho measured over the energy range of 1 to 135 MeV. The solid curve is our adiabatic coupled-channel (ACC) calculations using the optical-model parameters determined by fitting Cd and Pb (see text) and using $\beta=0.33$ for ^{165}Ho. The long-dashed curve is the no-coupling approximation with $\beta=0.33$ and the short-dashed curve is the same calculation but with $\beta=0$.

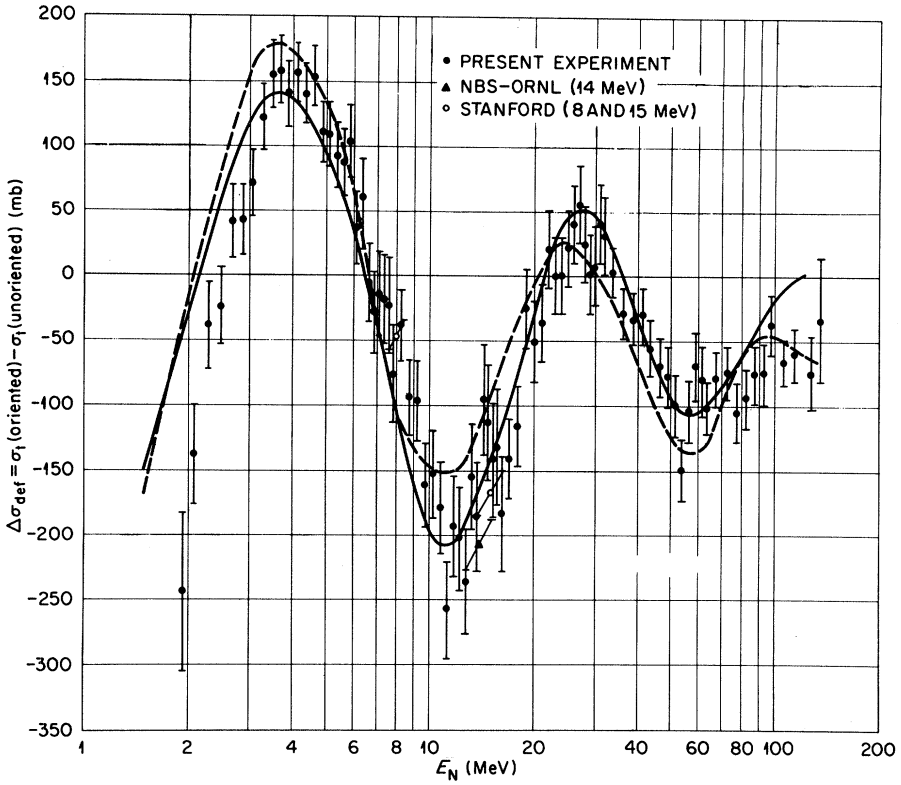

FIG. 6. $\Delta\sigma_{def}$ for ^{165}Ho measured over the energy range of 2 to 135 MeV for $T = 0.32$ K. The solid curve is the result of ACC calculations using the same optical-model parameters as those used in our σ_t calculation. The dashed curve was obtained from a semiempirical model (see text).

is deduced from the deviation of the seven individual sets of data about the mean as explained in Sec. II A. In order to compare the results for $\Delta\sigma_{def}$ from Ref. 4 (measured at 8 and 15 MeV) with ours, we multiplied their values by 30/25 since they had 0.25 for $B_2'/B_2(\max)$. These two points have been plotted in Fig. 6 and the agreement is very good. The comparison of our previous measurement of $\Delta\sigma_{def}$ at 14 MeV,[3] using an unmagnetized single crystal is not as straightforward, since the holmium nuclei were aligned perpendicular to the beam direction. However, we know that the shape of the holmium nucleus is almost pure quadrupole and that the contributions of the higher-order statistical tensors ($K = 4$ and 6) are relatively small, thus we need only concern ourselves with the rotation matrix $D^2_{00}(\theta) = P_2(\cos\theta)$ in changing the value for $B_2/B_2(\max)$ from the perpendicular to the parallel axis. Note that we dropped the prime on B_2, since in our 14-MeV work this quantity did not depend upon a magnetic model for the sample.[44] The value of $B_2/B_2(\max)$ was 0.54 ± 0.04, multiplying by $P_2(\cos\pi/2) = -\frac{1}{2}$ yields the value of -0.27 ± 0.02, and hence the value of $\Delta\sigma_{def}$ measured at 14 MeV is multiplied by $-30/27$. This is also plotted in Fig. 6, and as one can see the agreement is fairly good. Therefore we can conclude that our magnetic model for polycrystalline holmium metal enables us to calculate a reasonable value for B_2' at 0.32 K.

C. Temperature Dependence of $\Delta\sigma_{def}$

A complete series of data was also taken with the sample at 0.37 as well as at 0.94 K. The results for 0.37 K are shown in Fig. 7. One notes that the amplitude of the oscillations has decreased from that in Fig. 6. This is what we should expect since the value of $B_2'/B_2(\max)$ has decreased to 0.26 at 0.37 K. A measurement of the difference, $\delta(\Delta\sigma_{def})$, between the first maximum, $\Delta\sigma_{def}(\max)$, and the first minimum, $\Delta\sigma_{def}(\min)$, as a function of temperature should follow our $B_2'/B_2(\max)$ curve in Fig. 4 if our magnetic model is correct. This conclusion is independent of any nuclear models.

The position[45] and shape of the first maximum and minimum were fitted using the 0.32- and 0.37-K data. The difference was then calculated for these two sets of data as well as the 0.94-K set. These were plotted (bold points) as a function of $1/T$ in Fig. 8. Since we had some data as the sample was cooling down, we determined $\delta(\Delta\sigma_{def})$ for

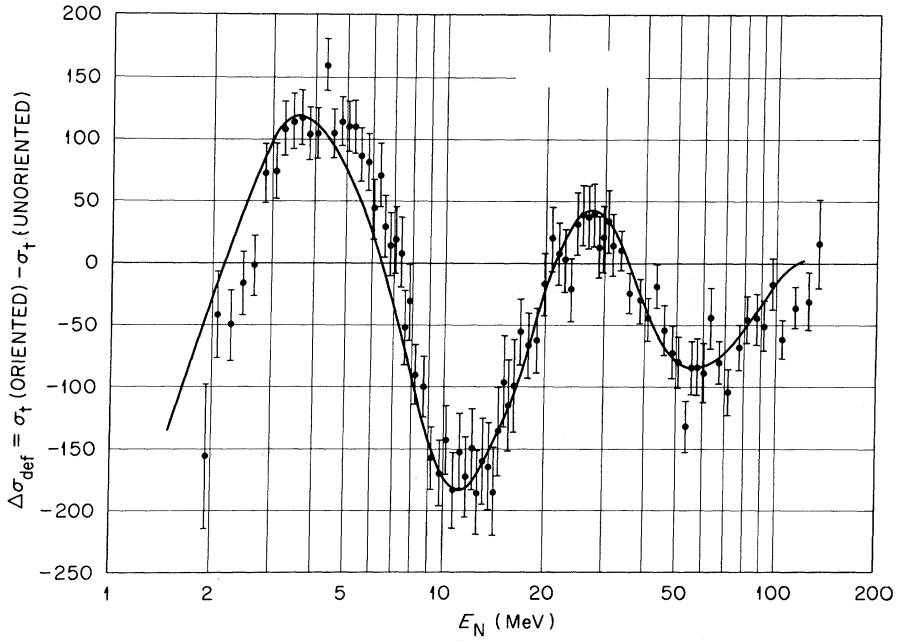

FIG. 7. $\Delta\sigma_{def}$ for ^{165}Ho measured at $T = 0.37$ K. The solid curve is our ACC results using the same optical-model parameters as before.

these and they are also plotted in Fig. 8. These latter points are less accurate statistically and temperaturewise. The solid line in Fig. 8 is our B_2'/B_2(max) curve. As the absolute magnitude of this curve depends upon a nuclear model, that is, we should have to relate the nuclear shape via some model to B_2'/B_2(max), we choose instead to normalize our curve to go through the 0.32-K point. As one can see, the curve goes exactly through

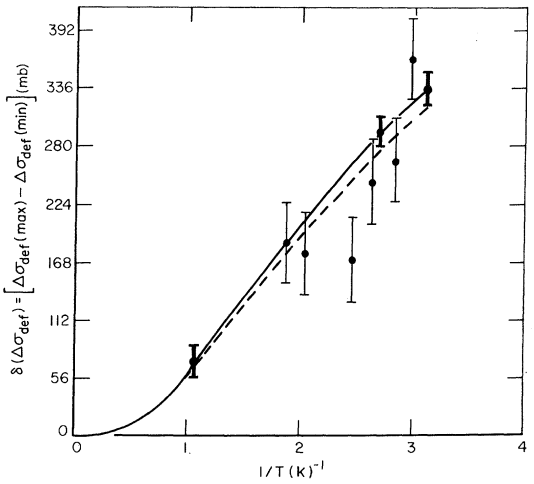

FIG. 8. Difference between the maximum (4.4 MeV) and minimum (12.6 MeV) of $\Delta\sigma_{def}$ versus the reciprocal of temperature. The three bold points are from our constant-temperature 0.32-, 0.37-, and 0.94-K data, whereas the remaining six points were taken as the sample was slowly cooling down. The solid curve is our B_2'/B_2(max) curve normalized to the 0.32-K point. The dashed curve is our ACC results and no normalization is needed in this case.

the other two bold points and thus it is immaterial which of the three bold points we use for the normalization. The other points are in relatively fair agreement with the curve. These data demonstrate that the nuclear-deformation effect goes as the B_2'/B_2(max) curve predicted by our magnetic model.

V. THEORETICAL ANALYSIS

A. Coupled-Channel Calculations

The experimental results for σ_t and $\Delta\sigma_{def}$ were analyzed using an optical-model potential of the form

$$V(r,\theta,\varphi) = -\frac{V}{1+e'} - \frac{iW}{1+\bar{e}'} - \frac{4iW_D\bar{e}'}{(1+\bar{e}')^2} - V_{so}(\vec{\sigma}\cdot\vec{l})\frac{r_\pi^{\,2}}{ar}\frac{e'}{(1+e')^2} \quad (5.1)$$

with

$$e' = \exp\{[r - R(\theta,\varphi,\theta_i)]/a\},$$

$$R(\theta,\varphi,\theta_i) = R_0[1+\beta Y_{20}(\theta')];$$

$$\bar{e}' = \exp\{[r - \bar{R}(\theta,\varphi,\theta_i)]/\bar{a}\},$$

$$\bar{R}(\theta,\varphi,\theta_i) = \bar{R}_0[1+\beta Y_{20}(\theta')],$$

$$R_0 = r_0 A^{1/3}, \quad \bar{R}_0 = \bar{r}_0 A^{1/3},$$

where the angles θ and φ refer to the space-fixed system, θ' to the body-fixed system, and θ_i stands for the Euler angles between these two systems.

In order to fix the parameters in (5.1), we first

fitted the optical-model predictions to the data[7,10] on the total cross section σ_t and the total reaction cross section σ_R of Cd and Pb. The fit was made over approximately the same range of neutron energies as our present work. This having been done, the calculation of σ_t and $\Delta\sigma_{def}$ for ^{165}Ho could be carried out with no further adjustment of parameters.

In calculating σ_t and σ_R for Cd and Pb, it was assumed that V and W_D decrease linearly with E_n, while W increases linearly; thus the three strengths V, W, and W_D are described by a set of six adjustable parameters. The other parameters a, $\bar{a}$, and $r_0=\bar{r}_0$ were left as energy-independent adjustable parameters while V_{so} was fixed at 7 MeV. Automatic search runs were made by Perey[46] to determine the above nine adjustable parameters [β in Eq. (5.1) is zero for Cd and Pb] and the best set of parameters obtained is the following (energies are in MeV and lengths in fm):

$$V=47.30-0.227E_n,$$
$$W=0.459+0.111E_n,$$
$$W_D=4.28-0.0414E_n\geq 0,$$
$$r_0=\bar{r}_0=1.211,$$
$$a=0.6812,$$
$$\bar{a}=0.6448,$$
$$V_{so}=7. \tag{5.2}$$

The fits to the total cross sections, Fig. 9, and that to the reaction cross sections, Fig. 10, are seen to be very good.

Having thus fixed the optical-model parameters, we can now proceed to the calculation of σ_t and $\Delta\sigma_{def}$ for ^{165}Ho. It is known,[47] however, that $\beta=0.33$ for ^{165}Ho, and this nonvanishing value of β makes the use of the simple optical-model calculation invalid contrary to the cases for Cd and Pb; we must use the coupled-channel calculations instead. However, since E_n is sufficiently high over most of the range of interest, we can use the (ACC) calculations,[48] which can be carried out much faster than the non-ACC calculations. As the derivation of the ACC equations and their solutions (in the form of the scattered waves and the cross sections) have been presented in detail in Sec. V of Ref. 3 and also in Sec. V of Ref. 48, the results are just quoted here. The expression for the total cross section, σ_t^{ACC}, is given by Eq. (7) of Ref. 3.

$$\sigma_t^{(ACC)}=\frac{4\pi}{k_1^2}\sum(2l'+1)\,\mathrm{Im}\sum_{ii'm_sm_s'M_1M_1'}a_{m_s}^{(i)}a_{m_s'}^{(i)*}b_{M_1}^{(i')}b_{M_1'}^{(i')*}Z^{(ACC)}_{m_sM_1,m_s'M_1';ll'} \tag{5.3}$$

with

$$Z^{(ACC)}_{m_sM_1,m_s'M_1';ll'}=\sum_{jlj'm_j}(ls0m_s|jm_s)(l's0m_s'|j'm_s')(-)^{m_s-\bar{m}_j}C^{\bar{m}_j}_{lj;l'j'}\times\sum_{JM_J}(I_1JK0|I_1K)(I_1JM_1M_J|I_1M_1')(jj'\bar{m}_j-\bar{m}_j|J0)(jj'm_s-m_s'|JM_j). \tag{5.4}$$

The meaning and derivation of the coefficients $a_{m_s}^{(i)}$ and $b_{M_1}^{(i')}$ in (5.3), which describe the orientation and/or polarization of the projectile and the target, respectively, have been explained in detail in Ref. 48. In particular, for an unpolarized neutron beam, we have

$$a_{1/2}^{(1)}=a_{-1/2}^{(2)}=\sqrt{\tfrac{1}{2}},\quad a_{-1/2}^{(1)}=a_{1/2}^{(2)}=0. \tag{5.5}$$

For the orientation of the target in the present experiment we describe $b_{M_1}^{(i)}$ in terms of the occupation number $P(N_1)$ by

$$b_{M_1}^{(N_1)}=[P(N_1)]^{1/2}\delta_{M_1N_1}. \tag{5.6}$$

For an unoriented ^{165}Ho nuclei, we have

$$b_{M_1}^{(N_1)}=\delta_{M_1N_1}/\sqrt{8}. \tag{5.7}$$

The total cross section for oriented and unoriented ^{165}Ho nuclei can now be obtained by using (5.6) and (5.7) in ACC calculations. However, in the latter the values of W and W_D were reduced by 20% compared with their corresponding values for Cd and Pb, since part of the absorption in the elastic channel is now taken into account explicitly in the inelastic scattering processes in the coupled excited states.[48]

The ACC calculations were performed by using the computer program JUPITOR-1.[49] The IBM 360/75 computer at Oak Ridge National Laboratory was used for most of the lower E_n, while for several higher values of E_n, where the computations take a longer time, the CDC 6600 computer at Brookhaven National Laboratory was used.[50] The theoretical σ_t and $\Delta\sigma_{def}$ obtained are compared with with experimental data in Figs. 5 and 6 and, as is seen, the agreement is very good (particularly for $\Delta\sigma_{def}$).[51] Because we used no adjustable param-

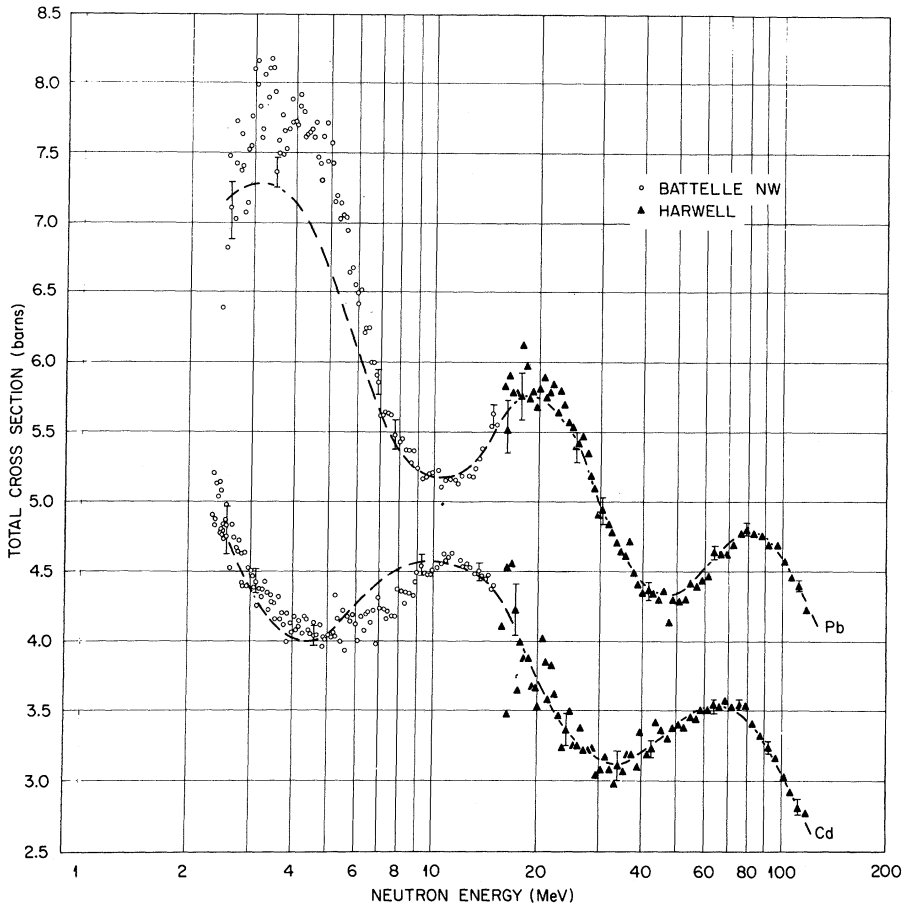

FIG. 9. Total neutron cross section for Cd and Pb covering an energy range of ~2 to 120 MeV. The dashed curves are least-squares fits which are used in determining the optical-model parameters (see text and Fig. 10.).

eters, these fits are significant and we may conclude that our data on σ_t and $\Delta\sigma_{def}$ can be accounted for very well by ACC.

B. Dependence of Theoretical Cross Sections on Various Parameters

Although good agreement is obtained with the experimental data, it will still be worthwhile to investigate how the results depend on (i) channel coupling, (ii) deformation parameter, and (iii) absorptive potential. These will each be treated separately. In all these investigations we used the optical parameters (5.2).

(*i*) *Effect of Channel Coupling*

As is seen in Ref. 48, in the treatment of the scattering from a deformed nucleus, the Woods-Saxon potential is expanded in terms of Legendre polynominals and then divided into diagonal and nondiagonal parts. The nondiagonal part of the potential gives rise to coupling between states in the target. In ACC, coupling between all the states in the ground-state rotational band are taken into account. However, one can also consider the approximation in which there is no coupling. Such a no-coupling approximation is nothing more than a conventional optical-model calculation (with the diagonal part of the potential modified from the original Saxon potential with $\beta_2 = 0$), and thus it

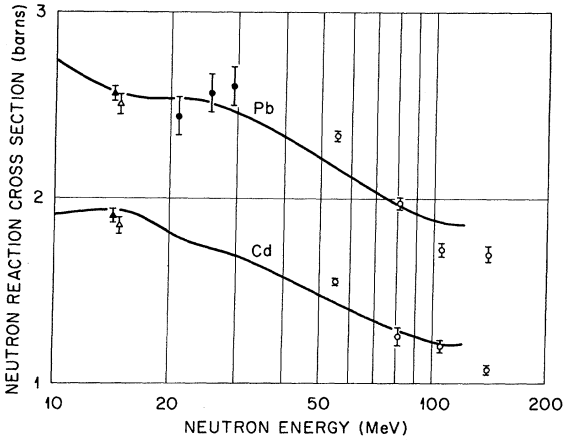

FIG. 10. Total neutron reaction cross section for Cd and Pb. The solid curves are least-squares fits which are used in determining the optical-model parameters (see text and Fig. 9).

can be performed very rapidly.

Using this approximation and setting the deformation parameter $\beta = 0.33$ as before, the total cross section σ_t is obtained and is as shown in Fig. 5 (long-dashed curve). Since no coupling is included, the strengths of the imaginary potentials were not reduced. As is seen in Fig. 5, the σ_t obtained for higher energies in the no-coupling approximation behaves fairly well with the σ_t obtained with coupling, but at lower energies the former deviates from the latter significantly and thus disagrees with experiment. Generally speaking, calculations with no coupling result in too large an amplitude of oscillation in σ_t as a function of E_n. Figure 5 (short-dashed curve) also contains σ_t with no coupling and with $\beta_2 = 0$; i.e., the σ_t obtained by means of a conventional optical-model calculation. Its general behavior is quite similar to that which was obtained with $\beta_2 = 0.33$ and without any coupling, except that the magnitude was slightly reduced for all E_n.

It is quite evident that these no-coupling calculations always give zero deformation effect.

(*ii*) *Effect of Deformation Parameters*

In ACC calculations, the strength of the coupling is specified by a deformation parameter β. Thus β is not a free parameter, since it can be determined by some other means. Nevertheless, it is instructive to investigate how σ_t and $\Delta\sigma_{def}$ depend on β. We chose to calculate these quantities at 4, 5, and 12 MeV, where $\Delta\sigma_{def}$ has a maximum or minimum value. The ACC calculations were performed using the parameters in (5.2) with the imaginary potential being reduced by 20% as before. The results of the calculations are shown in Figs. 11 and 12. As is seen in Fig. 11, at 5 and 12 MeV, σ_t increases as β increases, while at 4 MeV, σ_t decreases initially and then increases as β increases. This may be due to the shift in the peak of σ_t as β increases. Figure 12 shows $\Delta\sigma_{def}$ as a function of β. It is seen that $\Delta\sigma_{def}$ varies almost linearly with β for small β. However, as β exceeds 0.23, $\Delta\sigma_{def}$ begins to decrease. This means that a DWBA calculation, which predicts that σ_t is proportional to β, ceases to be valid for $\beta \geq 0.23$ as it gives too large a value for $\Delta\sigma_{def}$. For negative values of β, $\Delta\sigma_{def}$ changes sign. This implies that an oblate nucleus aligned similarly to the present experiment would have a minimum value of $\Delta\sigma_{def}$ at about 4 MeV and a maximum value at about 12 MeV.

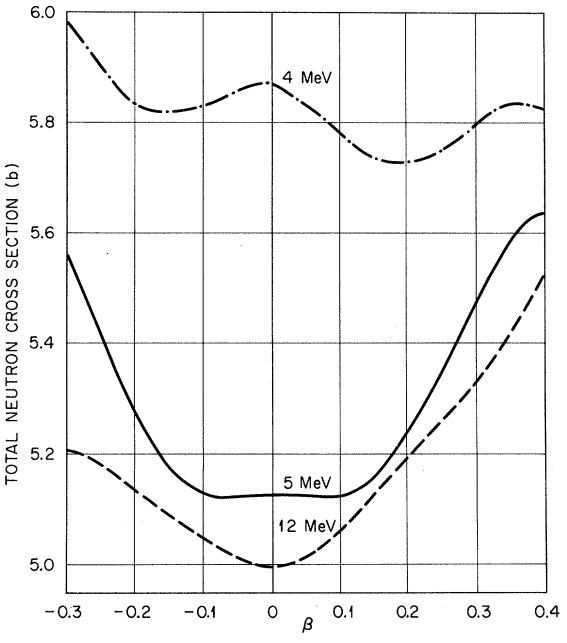

FIG. 11. Dependence of σ_t on β. These curves were obtained using the ACC and the same optical-model parameters as in our σ_t and $\Delta\sigma_{def}$ calculations.

(*iii*) *Effect of Change in Absorptive Potential*

There is no general rule on how much the absorptive potential should be reduced when a coupled-channel calculation is performed. The 20% reduction adopted in Subsec. A is based on our previous

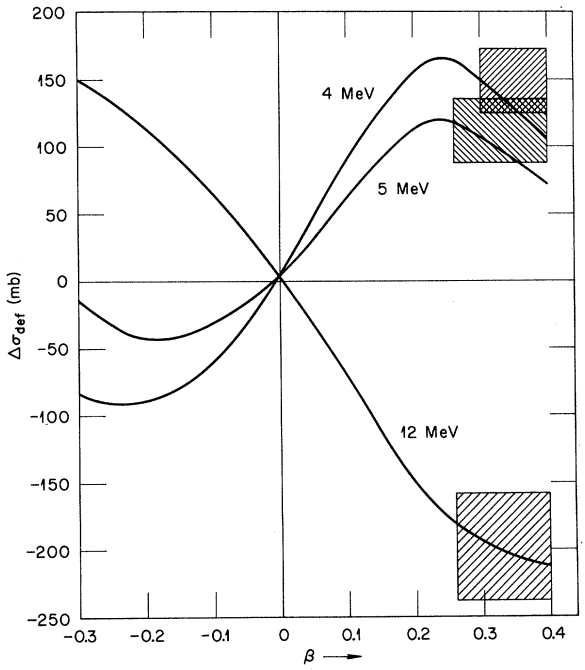

FIG. 12. Dependence of $\Delta\sigma_{def}$ on β. These curves were obtained using the ACC and the same optical-model parameters as in our σ_t and $\Delta\sigma_{def}$ calculations. The dashed areas are the experimental results for 0.32 K.

experiences in the analysis of the inelastic scattering of protons of 10–20 MeV.[48] Since the needed amount of reduction is expected to depend on the strength of the coupling and on the energy of the projectile, it would be worthwhile to see the effect of a change in W on σ_t and $\Delta\sigma_{def}$ for the present case. We therefore performed ACC with the strength of W unreduced for neutron energies up to 35 MeV. It is found that the difference between σ_t and $\Delta\sigma_{def}$ obtained with a reduced and unreduced W is small. The former gives a slightly larger amplitude of oscillation for $\Delta\sigma_{def}$ as a function of energy, and gives better agreement with experiment than does the latter.

C. Dependence of $\Delta\sigma_{def}$ on Nuclear Alignment

The ACC calculations for $\Delta\sigma_{def}$ can, of course, be repeated for different degrees of nuclear orientation, which come about by changing the sample temperature. Since we have experimental data for $T = 0.37$ K (Fig. 7), an ACC calculation was made for it also. We used the same values for the optical-model parameters as before, and the new values for the magnetic populations were obtained using (3.8), with (3.5) being used to determine the values of B'_K for 0.37 K. The results of this calculation are shown in Fig. 7 (solid curve), and as one can see the agreement is quite good over the entire energy range.

Rather than do another ACC calculation for the 0.94-K data it would be more useful to see if we can fit the $\delta(\Delta\sigma_{def})$-versus-temperature data shown in Fig. 8. ACC calculations were made for $\Delta\sigma_{def}$(max) at 4.4 MeV and $\Delta\sigma_{def}$(min) at 12.6 MeV as a function of temperature. Their differences are shown in Fig. 8 as the dashed curve along with the experimental results and the B'_2/B_2(max) curve. The agreement with the experimental points is quite good. It can be seen that the theoretical curve obtained from the ACC has almost the same shape as the B'_2/B_2(max) curve.[52] These results, although quite reasonable, are not evident from the ACC formalism, since it is done in terms of the magnetic populations directly and not in terms of the statistical tensors B'_K. Thus it would be instructive to see if we can recast the ACC in terms of the statistical tensors.

We define the density matrix in the usual way,

$$\rho'_{M_1M_1} = \sum_{i'} b_{M_1}^{(i')}\, b_{M_1}^{(i')*}, \tag{5.8}$$

and introduce the statistical tensors B_{KQ} by [53]

$$B_{KQ} = (2I_1+1)^{1/2} \sum_{M_1M_1'} \rho_{M_1M_1'} (-)^{K-I_1-M_1} (KQ\,|\,I_1I_1 - M_1M_1'). \tag{5.9}$$

Therefore the density matrix can be written in terms of the statistical tensors

$$\sum_{i'} b_{M_1}^{(i')}\, b_{M_1}^{(i')*} = (2I_1+1)^{-1/2} \sum_{KQ} B_{KQ} (-)^{K-I_1-M_1} (I_1I_1 - M_1M_1' | KQ). \tag{5.10}$$

Substituting (5.6) and (5.10) in (5.3) we have

$$\sigma_t^{(ACC)} = \frac{4\pi}{k_1^2} \sum_{l'} (2l'+1)\, \mathrm{Im} \sum_{m_s M_1 M_1' KQ} \tfrac{1}{2}(2I_1+1)^{-1/2} B_{KQ} (-)^{K-I_1-M_1} (I_1I_1 - M_1'|KQ)\, Z^{(ACC)}_{m_s M_1, m_s' M_1'; l'}. \tag{5.11}$$

Writing out $Z^{(ACC)}_{m_s M_1, m_s' M_1'; l'}$ explicitly as in (5.4), and after some simplifying we obtain

$$\sigma_t^{(ACC)} = \frac{4\pi}{k_1^2} \sum_{l'} (2l'+1)\, \mathrm{Im} \sum_{jlj'\bar{m}_j} \tfrac{1}{2}[(2j+1)(2l'+1)]^{1/2} (-)^{l'-j'-\bar{m}_j} C^{\bar{m}_j}_{lj;l'j'}$$

$$\times \sum_J (2J+1)^{-1/2} (I_1JK0\,|\,I_1K)(jj'\bar{m}_j - \bar{m}_j\,|\,J0) W(lsJj', jl')(ll'00\,|\,J0) B_{J0}. \tag{5.12}$$

The only terms which contribute to the sum over J are the ones with even J; this comes about because of the Clebsch-Gordan coefficient $(ll'00|J0)$ and parity considerations. For the case of the unoriented nuclei, all of the statistical tensors are zero except B_{00} which is always unity (normalization condition). We therefore obtain for $\Delta\sigma_{def}^{(ACC)}$ the following expression:

$$\Delta\sigma_{def}^{(ACC)} = \sigma_t(\text{oriented}) - \sigma_t(\text{unoriented}) = \frac{4\pi}{k_1^2} \sum_{l'} (2l'+1)\, \mathrm{Im} \sum_{jlj'\bar{m}_j} \tfrac{1}{2}[(2j+1)(2l'+1)]^{1/2} (-)^{l'-j'-\bar{m}_j} C^{\bar{m}_j}_{lj;l'j'}$$

$$\times \sum_{J=2,4,6} (2J+1)^{-1/2} (I_1JK0\,|\,I_1K)(jj'\bar{m}_j - \bar{m}_j\,|\,J0)(ll'00\,|\,J0) W(lsJj'; jl') B_{J0}, \tag{5.13}$$

where B_{J0} is the statistical tensor for the oriented case. In our experiment the orientation of the holmium nuclei is such that $B_{20} \gg B_{40} \gg B_{60}$. Furthermore, the factor $(2J+1)^{-1/2}(I_1 JK0 | I_1 K)$ in the summation over J is $\sqrt{\frac{7}{75}}$ for $J=2$, $\sqrt{\frac{7}{891}}$ for $J=4$ and $\sqrt{\frac{1}{5577}}$ for $J=6$. Therefore the contributions from $J=4$ and $J=6$ are small. This is borne out by the fact that the actual calculated ACC results shown in Fig. 8 are almost the same as the $B_2'/B_2(\max)$ curve, indicating almost a direct proportionality between $\Delta\sigma_{\rm def}$ and B_{20}. The small discrepancy between the dashed and solid curve is either due to the contribution of these two terms or comes about from the small energy shift in the maximum and minimum as explained in Ref. 45.

VI. INTERPRETATION OF $\Delta\sigma_{\rm def}$ USING THE BLACK-NUCLEUS MODEL AND THE NUCLEAR RAMSAUER EFFECT

Although, as we have seen in the previous section, the ACC accounts quite satisfactorily for the present σ_t and $\Delta\sigma_{\rm def}$ data, the calculation time on the computer becomes very large as the neutron energy is increased. It would, therefore, be worthwhile to develop another theoretical method to explain the present data. We shall show how the $\Delta\sigma_{\rm def}$ data can be explained quite well by using a semiempirical model which also gives a better physical insight into what is happening. This model makes use of the black-nucleus model, the nuclear Ramsauer effect, and the experimentally determined σ_t data.

If we compare the interaction between a neutron and an unaligned prolate nucleus to that when the nucleus is aligned with its symmetry axis along the neutron direction, the following two differences are noted; first, there is a decrease in the effective area of the nucleus, and second, there is an increase in the effective path length through the nucleus. The decrease in the effective area that the neutron sees can be calculated directly using the black-nucleus model, since this is just a geometrical effect. However, the increase in the effective path length for the neutron passing through the nucleus and its effect on the total cross section is more complicated. As we have pointed out in the introduction, the broad maxima and minima which appear in the total neutron cross sections have been successfully interpreted by Peterson[12] in terms of interference effects between the neutron wave going through and around the nucleus. In his analysis he showed that these effects were somewhat analogous to the electron Ramsauer effect, hence the name "nuclear Ramsauer effect." Since the position of the maxima and minima move towards higher neutron energy as the radius of the target nucleus is increased, we must take into account when we increase the effective path length through the nucleus.

Let us first calculate the reduction in the total neutron cross section using the black-nucleus model. It can be shown that the nuclear-deformation effect in terms of this model, $\Delta\sigma_{\rm def}^{(\rm BN)}$, is given by Eq. (22) of Ref. 3 with some slight modifications

$$\Delta\sigma_{\rm def}^{(\rm BN)} = \sigma_t\left(\frac{A_2}{A_0}\right)\frac{B_2}{B_2(\max)}\frac{5[3K^2 - I(I+1)]}{(I+1)(2I+3)}P_2(\cos\psi)\,. \tag{6.1}$$

We have neglected the B_4 and B_6 terms as they are insignificant. Here σ_t is the black-nuclear total cross section, A_0 and A_2 are integrals relating to the shape of the deformed nucleus, and ψ is the angle between the incident neutron and the orientation axis. Evaluating (6.1) for our experimental conditions, namely, $\beta = 0.33$, $B_2/B_2(\max) = 0.30$ ($T = 0.32$ K), $I = K = \frac{7}{2}$, and $\psi = 0$, yields[54]

$$\Delta\sigma_{\rm def}^{(\rm BN)} = -0.026\sigma_t\,. \tag{6.2}$$

Thus, there is a reduction in the total neutron cross section for holmium of 2.6% in terms of the black-nuclear model when we have 30% nuclear alignment. In order to calculate an absolute value for $\Delta\sigma_{\rm def}^{(\rm BN)}$, we have to evaluate σ_t. For a deformed nucleus, σ_t in the black-nucleus model is

$$\sigma_t = 2\pi(b+\lambda\!\!\!^{-})\left[\tfrac{1}{2}\left(b + \frac{a^2}{c}\sin^{-1}\frac{c}{a}\right) + \lambda\!\!\!^{-}\right], \tag{6.3}$$

where $2a$ is the length of the symmetry axis of the ellipsoid of revolution, $2b$ is the diameter of the largest circular cross section, and $c^2 = a^2 - b^2$. This equation reduces to the familiar $2\pi(a+\lambda\!\!\!^{-})^2$ when $a = b$. It can also be shown that up to fourth order in the parameter c/a, (6.3) is identical to the total cross section $2\pi(R+\lambda\!\!\!^{-})^2$ for a spherical nucleus with a radius R which has the same volume as our ellipsoid of revolution. Thus, the results given in (6.2), namely $\Delta\sigma_{\rm def}^{(\rm BN)}/\sigma_t = -0.026$, can be interpreted in another way. We can imagine an "equivalent" deformed nucleus which is aligned completely along the beam direction. There is a reduction in the geometrical area of 0.026, and hence the equivalent nucleus must have an axis larger by the factor 1.026 in order to have the same volume. Thus, we can say that the fractional increase in path length in the "equivalent nucleus" is given by

$$\Delta L/L = -\Delta\sigma_{\rm def}^{(\rm BN)}/\sigma_t\,. \tag{6.4}$$

Now let us calculate the energy shift in the maxima and minima due to the change in the effective path length when we align the deformed nucleus. We know[12] that the positions of the peaks are de-

termined by

$$(K-\kappa)L=C\,, \tag{6.5}$$

where

$$K=[2\mu(V+E)/\hbar^2]^{1/2},$$

$$\kappa=[2\mu E/\hbar^2]^{1/2},$$

L is the path length, and C is a constant. The positions of the valleys are given by an equation similar to (6.5) but with a different constant.

From (6.5) one obtains the shift in the energy of the peaks (or valleys) in terms of the change in path length by

$$\Delta E=\frac{2[(V+E)E]^{1/2}[(V+E)^{1/2}-E^{1/2}]}{(V+E)^{1/2}-E^{1/2}(1+dV/dE)}\cdot\frac{\Delta L}{L}\,. \tag{6.6}$$

We assume that (6.6) is applicable not only at the peaks and valleys, but everywhere. Such an assumption is reasonable because ΔE in this equation is a very smooth function of E.

If there were no reduction in the effective area seen by the neutron when a prolate nucleus is aligned with its symmetry axis parallel to the neutron beam, then the total cross section, $\sigma_t(E,$ oriented), for the aligned target at energy E would be equal to the total cross section, $\sigma_t(E-\Delta E,$ unoriented), for an unaligned target at energy $E-\Delta E$. However, from our previous analysis using the black-nucleus model, we know that there is a reduction in the cross section of 2.6% for our experimental situation. Thus, we have the approximation

$$\sigma_t(E,\text{ oriented})\cong\sigma_t(E-\Delta E,\text{ unoriented}) - 0.026[2\pi(R+\lambda\!\!\!^{-})^2]\,. \tag{6.7}$$

The nuclear-deformation effect in terms of this semiempirical model is

$$\Delta\sigma_{\rm def}^{(SE)}\cong\sigma_t(E-\Delta E,\text{ unoriented}) - 0.026[2\pi(R+\lambda\!\!\!^{-})^2]-\sigma_t(E,\text{ unoriented})\,. \tag{6.8}$$

Because ΔE is small (of the order of an MeV), we have

$$\Delta\sigma_{\rm def}^{(SE)}\cong\frac{-d\sigma_t(\text{unoriented})}{dE}\Delta E-0.026[2\pi(R+\lambda\!\!\!^{-})^2]\,. \tag{6.9}$$

To evaluate the first term in (6.9), we obtain $d\sigma_t$(unoriented)$/dE$ by drawing a smooth curve through the experimental points of the total cross section and measuring the slope of this smooth curve graphically. The resulting curve of $d\sigma_t$(unoriented)$/dE$ as a function of E is shown in Fig. 13. If one compares this with the experimental values of $\Delta\sigma_{\rm def}$ in Fig. 6, it is seen that $-\Delta\sigma_{\rm def}$ oscillates in approximately the same way as does our $d\sigma_t$(unoriented)$/dE$ curve, which is in qualitative agreement with our Eq. (6.9).

To obtain the energy shift, ΔE, we use the first relation of (5.2) namely,

$$V=47.30-0.227E\,, \tag{6.10}$$

and thus

$$dV/dE=-0.227\,. \tag{6.11}$$

The energy shift ΔE can be calculated from (6.6) by putting in 0.026 for $\Delta L/L$ and it is found to be a slowly varying function of energy. It increases from a value of 0.39 MeV for $E=1.5$ MeV to 1.9 MeV for $E=70$ MeV, and then decreases to 1.6 MeV for $E=130$ MeV.

$\Delta\sigma_{\rm def}^{(SE)}$ can then be obtained from (6.9), where we used $1.25A^{1/3}$ fm for R. The results from this model are shown in Fig. 6 as the dashed curve. The general features of the shape and oscillations of the experimental $\Delta\sigma_{\rm def}$ data are well reproduced by our semiempirical model over the entire energy range, thus indicating that the physical picture presented here is quite good.

VII. CONCLUSIONS

The experimental determination of the nuclear-deformation effect for ^{165}Ho, covering an energy range of ~2 to 135 MeV, has established both its oscillatory nature and sign reversal. The data are in very good agreement with the three discrete energy points 14 MeV,[3] and 8 and 15 MeV,[4] measured earlier. Recent measurements at 1.85, 4.50,

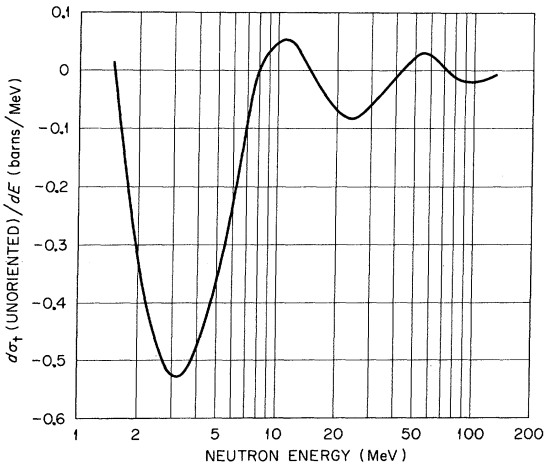

FIG. 13. The $d\sigma_t$(unoriented)$/dE$ versus E curve shown here was obtained by graphically differentiating our σ_t experimental data.

and 5.60 MeV by McCarthy *et al.*,[55] although not plotted in Fig. 6, are also in good agreement without data.

The theoretical predictions of the optical model using the ACC gave a very good fit to our $\Delta\sigma_{def}$ data, Figs. 6 and 7, and a relatively good fit to our σ_t data, Fig. 5. Although our fit of σ_t around 10 MeV is about 5% too high, it should be remembered that the optical-model parameters were solely determined by fitting the σ_t and σ_R data for the two adjacent spherical nuclei Cd and Pb, and then incorporating only the known quadrupole deformation parameter ($\beta = 0.33$) for ^{165}Ho in the ACC to obtain σ_t and $\Delta\sigma_{def}$.

We have also shown that our simple semiempirical model, which makes use of the black-nucleus model, the nuclear Ramsauer effect, and the experimental σ_t data, gives excellent agreement with our experimental results for $\Delta\sigma_{def}$. The question of whether the value predicted for $\Delta\sigma_{def}$ by the black-nucleus model alone, namely, $\Delta\sigma_{def}^{(BN)}$ given in (6.1), would agree with the experimental results at high energy (>100 MeV) cannot be answered in the present work, as the accuracy of our measurements at these energies is relatively poor. If the total cross section still oscillates, then the black-nucleus limit will not be reached. Although very little data exist for total neutron cross sections in the energy region above 120 MeV, there is some indication[12] that there are only three maxima and minima appearing in σ_t and hence, perhaps, the black-nucleus limit is reached.[56]

Although the value predicted by (6.1) for $\Delta\sigma_{def}^{(BN)}$ does agree with the experimental $\Delta\sigma_{def}$ at certain discrete energies, namely, where the monotonically decreasing curve of $\Delta\sigma_{def}^{(BN)}$ crosses our oscillating experimental $\Delta\sigma_{def}$ data, this agreement is fortuitous. The result of Inopin,[57] showing that the 15-MeV result of Fisher *et al.*[4] is in good agreement with the black-nucleus model, is slightly in error and therefore is not one of these fortuitous agreement points.

Finally, we have shown in measuring the temperature dependence of $\Delta\sigma_{def}$, Fig. 8, that the excellent agreement with our calculated values for $B_2'/B_2(\max)$ is consistent with ^{165}Ho being almost a pure quadrupole-shaped nucleus as concluded by Hendrie *et al.*[16]

ACKNOWLEDGMENT

We wish to thank Dr. R. P. Hudson, Dr. B. Rose, and Dr. A. E. Taylor for their continued encouragement and support of this work. The assistance of P. H. Bowen, G. C. Cox, P. J. Clemens, R. B. Dove, and the staff of the Harwell synchrocyclotron is deeply appreciated. We would like to thank Dr. F. Perey for his studies in the search of the optical-model parameters. We are indebted to Dr. A. Prince and Dr. P. S. Tu for assistance in performing the ACC with the CDC 6600 computer at the Brookhaven National Laboratory. One of us (H.M.) would like to acknowledge the kind hospitality of the Atomic Energy Research Establishment at Harwell, and the many people there whose help made it possible to carry out these measurements in a very short time.

---

*A short report of this work has been published: H. Marshak, A. Langsford, C. Y. Wong, and T. Tamura, Phys. Rev. Letters 20, 554 (1968).

†Work done under the auspices of the U. S. Atomic Energy Commission.

[1]The fact that it can be easily oriented has also made it a very useful target in the search for a spin-spin coupling in the neutron-nuclear interaction, in the study of the charge form factor using high-energy electrons, in studying details about the giant-dipole resonance, and finally in making spin assignments of $l = 0$ neutron resonances.

[2]R. Wagner, P. D. Miller, T. Tamura, and H. Marshak, Phys. Rev. 139, B29 (1965).

[3]H. Marshak, A. C. B. Richardson, and T. Tamura, Phys. Rev. 150, 996 (1966).

[4]T. R. Fisher, R. S. Safrata, E. G. Shelley, J. McCarthy, S. M. Austin, and R. C. Barrett, Phys. Rev. 157, 1149 (1967).

[5]G. L. Visotskii, E. V. Inopin, and A. A. Kresnin, Zh. Eksperim. i Teor. Fiz. 36, 574 (1959) [transl.: Soviet Phys. – JETP 9, 398 (1959)]; see S. Z. Drozodov, Zh. Eksperim. i. Teor. Fiz. 28, 734 (1955) [transl.: Soviet Phys. – JETP 1, 588 (1955)]; and also Ref. 3.

[6]For a deformed nucleus we use for the radius, R, that of a spherical nucleus of equal volume.

[7]D. G. Foster, Jr., and D. W. Glasgow, Nucl. Instr. Methods 36, 1 (1965); and to be published.

[8]K. T. R. Davies, G. R. Satchler, R. M. Drisko, and R. H. Bassel, Nucl. Phys. 44, 607 (1963).

[9]T. Tamura, Rev. Mod. Phys. 37, 679 (1965).

[10]P. H. Bowen, J. P. Scanlon, G. H. Stafford, J. J. Thresher, and P. E. Hodgson, Nucl. Phys. 22, 640 (1961).

[11]J. D. Lawson, Phil. Mag. 44, 102 (1953).

[12]J. M. Peterson, Phys. Rev. 125, 955 (1962).

[13]K. W. McVoy, Phys. Letters 17, 42 (1965); Ann. Phys. (N.Y.) 43, 91 (1967).

[14]V. Franco, Phys. Rev. 140, B1501 (1965).

[15]Throughout this paper we are concerned with the nuclear form factor and not the charge form factor.

[16]D. L. Hendrei, N. K. Glendenning, B. G. Harvey, O. N. Jarvis, H. H. Duhm, J. Saudinos, and J. Mahoney,

Phys. Letters 26B, 127 (1967).

[17]And then only on the even-order orientation parameters.

[18]J. P. Scanlon, G. H. Stafford, J. J. Thresher, and P. H. Bowen, Rev. Sci. Instr. 28, 749 (1957).

[19]The even-order orientation parameters are associated with nuclear alignment and the odd-order parameters with nuclear polarization.

[20]The terminology which seemed to evolve (but not universally) is that the entire system (cryostat, pumps, vacuum gauges, etc.) is called a refrigerator, and the part which contains the cryogenic liquids and where the actual cooling takes place is called the cryostat.

[21]This design, which is sometimes called a bent cryostat, has some novel features which justify the added complexity in construction. The two most important are that one can use a high-field, large-bore superconducting solenoid rather than a lower-field, split superconducting solenoid with limited sample volume and that the sample can be changed quite easily. It would be fairly simple to incorporate this type of construction into the design of a ^{3}He-^{4}He dilution cryostat.

[22]One would need a relatively large-cooling-capacity refrigerator (either a ^{3}He-^{4}He dilution or magnetic) to cool a sample of the size of ours.

[23]Their field was first turned up to 22 kOe and then lowered to 18 kOe, thus affording them safer operation in the persistent mode, since the magnet was in the vacuum space.

[24]R. S. Safrata, T. R. Fisher, and E. G. Shelley, J. Appl. Phys. 37, 4869 (1966).

[25]Some idea of the cooling involved can be obtained by calculating how much copper we could equivalently cool in place of our holmium sample. This turns out to be 2.1 tons!

[26]Using Indalloy No. 2 solder (Indium Corporation of America) without any flux.

[27]All of the copper parts of the cryostat are made from high-purity oxygen-free copper.

[28]The ^{3}He refrigerator is known to operate at about 2 mW between 0.9 and 0.3 K. The 1.5 h needed to cool our sample represents a cooling rate of 1.4 mW, which indicates that we are making fairly good contact with our holmium sample.

[29]Although one could use extremely thin windows with this geometry, no effort was made to do so, since the experimental conditions did not warrant it.

[30]All the inside windows are removed and the outside windows replaced by transparent ones; thus the holmium can be viewed directly. The cryostat can then be cooled to 77 K, at which temperature 97% of the vertical shrinkage (4.5 mm) has taken place, and then the sample can be lined up with the collimator.

[31]V. B. Belionin, Opt. Spectrosc. 5, 236 (1958); J. E. Gordon, C. W. Dempesy, and T. Soller, Phys. Rev. 124, 724 (1961); H. Postma, H. Marshak, V. L. Sailor, F. J. Shore, and C. A. Reynolds, Phys. Rev. 126, 979 (1962); B. Bleaney, J. Phys. Soc. Japan Suppl. 17, 435, (1962); O. V. Lounasmaa, Phys. Rev. 128, 1136 (1962); H. van Kempen, A. R. Miedema, and W. J. Huiskamp, Physica 30, 229 (1964); G. Brunhart, H. Postma, and V. L. Sailor, Phys. Rev. 137, B1484 (1965).

[32]B. L. Rhodes, S. Legvold, and F. H. Spedding, Phys. Rev. 109, 1547 (1958); D. L. Strandburg, S. Legvold, and F. H. Spedding, Phys. Rev. 127, 2046 (1962); D. L. Strandburg, Ph.D. dissertation, Iowa State University, 1962 (unpublished); W. C. Koehler, J. W. Cable, M. K. Wilkinson, and E. O. Wollan, Phys. Rev. 151, 414 (1966).

[33]H. van Kempen, A. R. Miedema, and W. J. Huiskamp, Physica 30, 229 (1964).

[34]D. L. Strandburg, S. Legvold, and F. H. Spedding, Phys. Rev. 127, 2046 (1962).

[35]J. J. Rhyne, S. Foner, E. J. NcNiff, Jr., and R. Doclo, J. Appl. Phys. 39, 892 (1968); and S. Foner, private communication.

[36]Recently one has been done using a single-crystal sample; M. A. Kelly, B. L. Berman, R. L. Bramblett, and S. C. Fultz, Phys. Rev. 179, 1194 (1969).

[37]E. G. Shelley, Ph.D. thesis, Stanford University, 1966 (unpublished).

[38]These measurements were kindly made for us by Dr. S. Foner of the National Magnet Laboratory.

[39]It should be kept in mind that the model is clearly an oversimplification of the magnetization process in polycrystalline holmium metal; for example, magnetization measurements show that the canting angle is not fixed, but does change very slowly as the applied field is increased. Corrections for this, although small, would tend to increase the value of the magnetization over that which our model predicts. This is borne out by the experimental measurements; at 60 kG the magnetization is already slightly larger (0.835) than the value (0.826) predicted for the intermediate-saturation plateau by our model. The observed intermediate-saturation plateau is not really a plateau, but has a slight slope as one should expect, since as we increase the field (hundreds of kG) the moments should line up with the field.

[40]To illustrate the fact that B_2' is so model dependent, imagine a magnetic model (which is not the case for holmium) which had all the atomic spins at an angle of $54°45'$ to the applied-field direction, then B_2' would zero, since $P_2(\cos 54°45') = 0$.

[41]The sample was magnetized 10 times before any data were taken, in order to insure that we were on the top branch of the hysteresis loop. Data were also taken at 55 kOe with no apparent change in $\Delta\sigma_{\text{def}}$.

[42]Some idea of the uncertainty in the $K=2$ term can be obtained by comparing our previous result of $\Delta\sigma_{\text{def}}$ at 14 MeV (using an unmagnetized single crystal) with our present measurement of $\Delta\sigma_{\text{def}}$ at the same energy. This is discussed in Sec. IV.

[43]S. Kobayashi, H. Kamitsubo, K. Katori, A. Uchida, M. Imaizumi, and K. Nagamine, J. Phys. Soc. Japan 22, 368 (1967).

[44]One knows, with a reasonable degree of certainty, the distribution of atomic moments in an unmagnetized single crystal. See Refs. 2 and 3.

[45]This turned out to be 4.4 MeV for the maximum and 12.6 MeV for the minimum. The remaining data were analyzed by keeping the position of the maximum and minimum fixed. This introduces a small error, since the positions of the maxima and minima change slightly as the degree of nuclear orientation changes.

[46]F. J. Perey, private communication.

[47]B. Elbek, *Determination of Nuclear Transition Probabilities by Coulomb Excitation* (Ejnar Munksgaard Forlag, Copenhagen, Denmark, 1963); M. Danos and W. Greiner, Phys. Letters 8, 113 (1964); E. Ambler, E. G. Fuller, and H. Marshak, Phys. Rev. 138, B117 (1965).

[48]T. Tamura, Rev. Mod. Phys. 37, 679 (1965).

[49]T. Tamura, Oak Ridge National Laboratory Report No. ORNL-4152, 1967 (unpublished).

[50]We are indebted to Dr. A. Prince and Dr. P. S. Tu of the Brookhaven National Laboratory for performing these calculations with the CDC 6600 computer.

[51]In calculating $\Delta\sigma_{\rm def}$, the values for $P(N_1)=P'_M$ are determined from (3.8) and using the B'_K for $T=0.32$ K from Table I.

[52]This small difference might be due to the energy shift of the maximum and minimum as discussed in Ref. 42. For ease in calculation, the positions of the maximum and minimum were fixed by the experimental data and not by the ACC.

[53]We have dropped the prime from this more general definition of the statistical tensors. Our B'_K are, therefore, the same as these when $Q=0$.

[54]In our previous short report on this work we inadvertently used $\beta=0.3$ instead of $\beta=0.33$, thus obtaining only a 2.4% reduction instead of the 2.6% reported here.

[55]J. S. McCarthy, T. R. Fisher, E. G. Shelley, R. S. Safrata, and D. Healey, Phys. Rev. Letters 20, 502 (1968).

[56]It would be worthwhile to extend these measurements to both higher energies (~200 MeV) and lower energies (< 2 MeV). These, of course, should be done using a similar experimental setup (namely, pulsed machines and time-of-flight techniques) so that one can cover the energy range continuously.

[57]E. V. Inopin, Yadern. Fiz. 5, 1008 (1967) [transl.: Soviet J. Nucl. Phys. 5, 719 (1967)]; Eq. (18) in this paper is slightly in error.

PHYSICAL REVIEW C VOLUME 2, NUMBER 5 NOVEMBER 1970

Gamma-Gamma Directional Correlations in the Decay of Nd^{147}

Nick Blaskovich, Jr.,* and Atam P. Arya
Department of Physics, West Virginia University, Morgantown, West Virginia 26506
(Received 15 May 1970)

A 10-cc coaxial Ge(Li) detector and a 2-in.×2-in. NaI(Tl) detector were used in conjunction with a multichannel coincidence configuration to investigate the following γ-γ directional correlations in the decay of 11.1-day Nd^{147}: 319-91, 398-91, 440-91, 121-319, and 276-319 keV. Using the well-established values of $\frac{7}{2}$ and $\frac{5}{2}$ for the ground and 91-keV levels, respectively, and an admixture of $(1.6\pm0.4)\%$ $E2$ for the 91-keV transition, this experiment favored the following spin assignments to the various levels: 410 $(\frac{3}{2})$, 489 $(\frac{5}{2})$, 531 $(\frac{5}{2})$, and 686 keV $(\frac{5}{2})$. The $M1+E2$ multipolarity mixtures obtained, which are in agreement with nuclear-orientation and internal-conversion measurements reported by previous investigators, for each of the respective γ transitions are: 121 $(1.5\pm0.5)\%$ $E2$, 276 $(\sim1)\%$ $E2$, 319 $(11\pm2)\%$ $E2$, 398 $(3\pm2)\%$ $E2$, and 440 keV $(27\pm7)\%$ $E2$. A 310-keV γ ray proposed by several investigators was directly observed in the Ge(Li) spectrum; measurements indicate that this peak decays with the half-life of Nd^{147}.

I. INTRODUCTION

A considerable number of investigations[1-14] have been made of the decay of 11.1-day Nd^{147} to Pm^{147}. The locations of excited levels of Pm^{147} at 91, 410, 489, 531, and 686 keV, as depicted in Fig. 1 have unambiguously been established. The introduction of a level at 680 keV has been proposed by Hill and Wiedenbeck[1] which deexcites to the 91-keV state via a 589-keV γ emission or to the ground state via a 680-keV γ emission. Studies by Canty and Conner[6] also support the inclusion of such a level. Gunye, Jambunathan, and Saraf[3] and Spring[4] have proposed a 720-keV level depopulating via a 310-keV transition to the 410-keV level.

The ground state of Nd^{147} has been measured by paramagnetic-resonance studies[7] and the atomic-beam method,[8] which consistently assign the spin value $\frac{5}{2}^-$. The spin of the Pm^{147} ground state has been measured by Klinkenberg and Tomkins[9] as $\frac{7}{2}^+$ corresponding to the $g_{7/2}$ shell-model state.

The 91-keV excited state of Pm^{147} is populated from the ground state of Nd^{147} via β decay with a logft value[10] of 7.4, indicating that this β transition is first forbidden. This subsequently limits spin assignments to the 91-keV level to $\frac{3}{2}^+$, $\frac{5}{2}^+$, or $\frac{7}{2}^+$. The predominantly $M1$ character of the 91-keV transition[1,2] eliminates the $\frac{3}{2}^+$ possibility. Nuclear-orientation experiments by Westenbarger and Shirley[5] exclude a $\frac{7}{2}^+$ assignment because it results in an $E2$ admixture of 48% or more for the 91-keV γ ray. By internal-conversion measurements, Ewan[2] has estimated this admixture as ~1%, while Westenbarger and Shirley affix an upper limit of 2% $E2$ to this transition. Reinterpretation of the Oxford directional and polarization data[11] by Westenbarger and Shirley[5] yields the same results. Thus this level is assigned a spin of $\frac{5}{2}^+$.

On the basis of relative photon intensities studied with a Ge(Li) detector, Hill and Wiedenbeck[1] were